Machine Learning-Based Real-Time Walking Activity and Posture Estimation in Construction With a Single Wearable Inertial Measurement Unit

Siyu Chen, Chunchu Zhu, *Student Member, IEEE*, Xunjie Chen, *Student Member, IEEE*, and Jingang Yi, *Senior Member, IEEE*

***Abstract*—Construction workers regularly perform walking locomotion on level and inclined surfaces. It is critical to detect walking activity and estimate body postures in real time for monitoring workers' safety and health conditions. This article presents a machine learning-based framework for real-time activity detection and posture estimation during human walking on level and sloped terrains using a single wearable inertial measurement unit (IMU). The framework integrates recurrent neural networks with Gaussian process dynamical models to achieve accurate predictions of walking activity, floor slope angles, and workers' turning angles and full-body limb joint angles estimation in real time. The proposed design offers a streamlined, cost-effective solution with significant advantages over multi-sensor systems. Extensive experiments of different walking activities on level and sloped surfaces are conducted to validate and demonstrate the design. The proposed algorithm detects gait activities with 96% accuracy, the estimated human limb joint angle errors are within 11 deg, the predicted turning angles have an error less than 16 deg and the end-to-end detection latency is within 21 ms using only one single IMU attached to the human shank.**

***Note to Practitioners*—Construction workers exert intense physical effort, and they experience serious safety and health risk in hazardous, dynamic working environments. As a result, the construction industry is one of the highest-risk industrial sectors in most countries. Real-time monitoring of workers' walking gait plays a critical role in construction safety. Wearable IMUs are particularly attractive for walking activity recognition because they are small, inexpensive, and non-intrusive. This study aims to develop machine learning-enabled, real-time IMU-based walking activity recognition and full-body posture and floor slope angle estimation. The main approach is built on long short-term memory (LSTM)-based recurrent neural networks and a manifold learning method to process time-series data from the IMU to predict human motion. The LSTM model achieves over 96% accuracy to classify various walking activities on different floor slopes. Additionally, the design also estimates human limb joint angles, floor slope angle and the worker's body turning angle. A noteworthy aspect of the detection system is the minimal detection latency of 18 ms, ensuring the reliability and effectiveness of real-time monitoring and evaluation. This feature is particularly beneficial for immediate feedback and intervention systems that help protect workers from work-related injuries. The simplicity and efficiency of using a single IMU are attractive for a practical solution for real-time automation applications in dynamic environments.**

***Index Terms*—Posture estimation, activity detection, construction workers, construction automation, wearable inertial sensors.**

I. Introduction

CONSTRUCTION workers are exposed to serious safety and health risks in hazardous, dynamic environments. Walking on level and sloped surfaces is one of the most common gaits in construction trades (e.g., roofers, scaffold builders, etc.) It is critical to monitor workers' activity and body posture in real time for safety and health conditions assessment [1]. Visual cameras, inertial measurement units (IMUs) and motion sensors are among the most widely used sensing systems for activity tracking, monitoring and evaluation [2]. For example, computer vision techniques are used to extract features from images or videos for pose estimation or body landmark detection [3]. Wearable sensor networks, such as IMUs, enable posture estimation and activity recognition even without direct visual observation [4]. Wearable IMUs are particularly attractive for gait detection and posture estimation in construction because they are small-size, low-cost, and non-intrusive [5]. In [6], two IMUs were attached to the back of the helmet and the worker's back for head, neck and trunk inclination estimation. In [7], eight IMUs were attached to the trunk and limbs to detect gaits and motion of construction workers. In [8], 17 IMUs were used to identify poses of masonry workers using support vector machines. Comparison results of various IMU locations on the human body segments were reported in [9]. Inertial sensor-based gait classification and detection were also applied to human kneeling, squatting and foot slip activities (e.g., [10], [11], [12], [13], [14]). Comparing with vision cameras, IMUs do

Received 16 October 2024; revised 15 February 2025 and 24 April 2025; accepted 18 May 2025. Date of publication 27 May 2025; date of current version 6 June 2025. This article was recommended for publication by Associate Editor M.-H. Hung and Editor G. Fortino upon evaluation of the reviewers' comments. This work was supported in part by US NSF under Award IIS-2026613 and Award CMMI-2222880. An earlier version of this paper was presented in part at the 2021 IEEE/ASME International Conference on Advanced Intelligent Mechatronics, Delft, The Netherlands, July 12–16, 2021 [DOI: 10.1109/AIM46487.2021.9517592]. *(Siyu Chen and Chunchu Zhu contributed equally to this work.) (Corresponding author: Jingang Yi.)*

This work involved human subjects or animals in its research. Approval of all ethical and experimental procedures and protocols was granted by the Institutional Review Board at Rutgers University under Application No. Pro2022001364.

Siyu Chen was with the Department of Mechanical and Aerospace Engineering, Rutgers University, Piscataway, NJ 08854 USA. He is now with MathWorks, Inc., Natick, MA 01760 USA (e-mail: siyu.chen@rutgers.edu).

Chunchu Zhu, Xunjie Chen, and Jingang Yi are with the Department of Mechanical and Aerospace Engineering, Rutgers University, Piscataway, NJ 08854 USA (e-mail: chunchu.zhu@rutgers.edu; xunjie.chen@rutgers.edu; jgyi@rutgers.edu).

Digital Object Identifier 10.1109/TASE.2025.3573966

not need any infrastructure support and can perform under various weather and terrain conditions [5].

Few of the aforementioned studies focus on wearable IMU-based, real-time applications. In [15], a real-time gait event detection was presented to capture walking gait events over level and inclined floors and staircases using a single IMU. Similar real-time walking gaits detection approaches were also reported in [16] and [17] for periodic gait movement using machine learning methods. For gait detection of non-periodic human movements, the work in [7] and [14] used a set of wearable IMUs on human limbs and trunk to monitor construction workers' gait activities. In [13], seven wearable IMUs were used to detect sudden foot slip during walking. Wearable IMU-based human activity detection was also presented in [18] for real-time applications. The work in [19] explored using IMUs for horse limb lameness detection and pose estimation in real time.

Floor slope information is important for assessing safety and ergonomics of construction workers. Sloped surfaces directly influence the postures and movements of construction workers. Prolonged stance and walking gaits on sloped surfaces can potentially lead to work-related musculoskeletal disorders (WMSDs) or even injuries [20]. Empirical studies have demonstrated a significant correlation between slope angles and the incidence of musculoskeletal disorders. Emerging technologies such as wearable sensing and exoskeletons appear to be a promising intervention to mitigate the WMSDs in construction [20], [21]. By harnessing accurate slope estimation, wearable exoskeletons have been demonstrated to provide dynamic, context-sensitive support, thereby mitigating the ergonomic risks associated with walking on sloped surfaces [22], [23]. Real-time slope angle estimation and human walking activities detection were conducted with IMUs and encoders in [24].

Machine learning techniques were used in recent years for human activity detection and posture estimations [25], [26]. Deep convolutional neural networks and long short-term memory networks (CNN-LSTM) architectures were used to improve human activity recognition [27], [28]. Diffusion models were also used in 3D human pose estimation from single 2D observations [29], [30]. Hybrid and ensemble learning approaches have significantly improved performance of gait and activity recognition systems. Integrated CNN and LSTM architectures effectively capture both spatial and temporal dynamics, enabling robust classification of complex motion patterns [31]. Furthermore, compressed deep neural networks have been employed for lightweight implementations tailored for real-time rehabilitation robotics applications [32]. However, few of the above-mentioned machine learning-based methods focus on real-time applications.

In this paper, we present a real-time walking activity detection and pose estimation scheme on level and sloped floor surfaces using only a single IMU. We take advantage of the periodical motion property of walking gaits to predict full body motions through a low dimensional representation. An LSTM approach is used to detect the walking gaits and predict the floor slope angle and human turning angle. A learned motion manifold is then constructed using the walking activity information. The pose estimation is built on the learned motion walking manifold and the IMU measurements. We use the Gaussian process dynamic model (GPDM) to construct the human motion manifold [33]. Similar to [34], due to the periodic feature in human walking, the learned GPDM is represented as a closed-curve (manifold) in latent space and a phase variable is used to parameterize the GPDM model to predict the joint angles in real time. Compared with traditional kinematic-based models in gait estimation, GPDM shows improved accuracy and fast computation.

The proposed integrated activity detection and posture estimation provides a holistic assessment of worker safety and ergonomics in demanding construction environments. This integration design also simplifies the system architecture, reduces sensor requirements, and improves real-time response, making it highly practical for real-world applications in construction. Extensive human experiments are conducted on level and sloped surfaces that represent roof workers in construction. The experimental results demonstrate the efficacy and effectiveness of the design. By using only one single IMU, the synchronization and sensing latency between sensors are minimized and this reduces the design complexity. This property is particularly attractive for monitoring worker's activity and posture in real time since that it is inconvenient to wear a complex monitoring system in construction work site.

In contrast to prior works that require multiple sensor inputs (e.g., IMUs on various body parts, goniometers (GONs), electromyography (EMG), etc.), the proposed framework utilizes a single shank-mounted IMU. Despite its simplicity, the main contribution of this work also lies in the novel integration of LSTM and GPDM for real-time walking activity detection and limb posture estimation as well as floor slope and turning angles prediction. This approach significantly advances real-time worker gait monitoring in physically demanding environments such as construction sites, reducing system complexities while achieving high classification accuracy across diverse floor slopes. The use of GPDM for real-time limb joint angle prediction provides a potential enabling tool for integrated wearable robotic systems to mitigate the risk of WMSDs in construction. Compared with the previous conference presentation [35], the current work presents a comprehensive study, introducing new elements such as the estimation of human turning angles. The experiments are extensive, incorporating an analysis of the algorithm's performance on interpolated slopes and its adaptability to alternative datasets. Furthermore, the presented work offers an in-depth discussion and comparison of the algorithms with other reported results. These results highlight the significance of the proposed framework for enhancing safety and ergonomics in construction, which are not presented in [35].

The remainder of the paper is organized as follows. We present the problem statement in Section II. Section III discusses the experiment configuration and data collection. Section IV presents the walking activity detection and posture estimation algorithms. Experimental results are presented in Section V, followed by discussions in Section VI. We finally summarize the conclusion in Section VII.

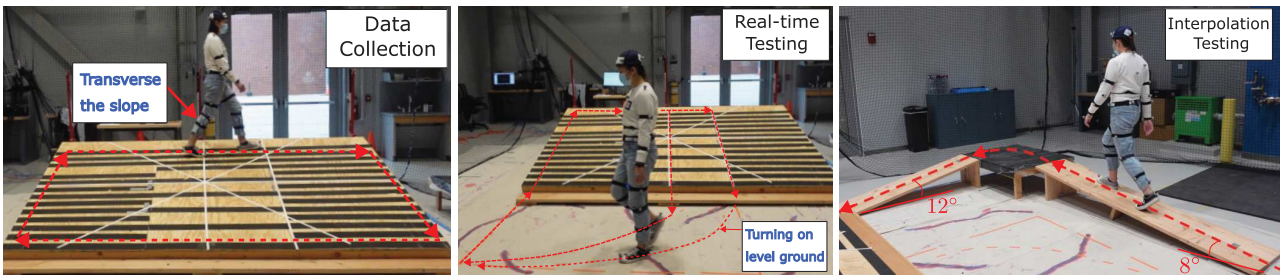

(a) (b) (c)

Fig. 1. Laboratory experimental setup mimicking roofer trade in construction, including different walking setup on variable sloped wooden structure. (a) Experimental setup for training data collection. (b) Real-time walking test on different slope angles and turning radius. (c) Experimental test for walking on the sloped surfaces with angles that were not among the training data.

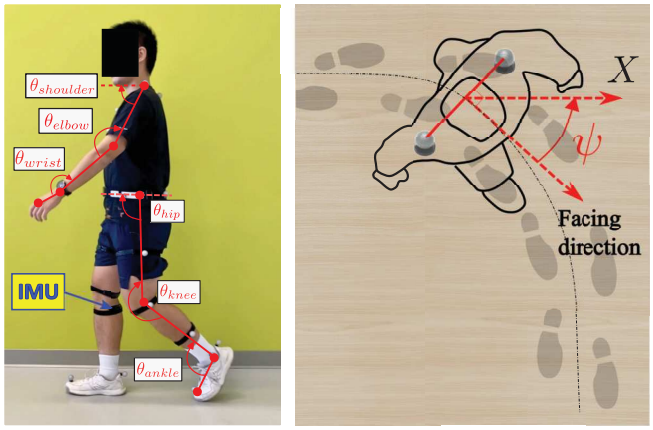

(a) (b)

Fig. 2. (a) Human body joint angles in the sigittal plane with a single wearable IMU and optical markers in experiments. (b) Illustrative schematic of the human turning angle ψ on the level and sloped surfaces.

II. Problem Statement

We consider human walking gaits on level and sloped floor surfaces as shown in Fig. 1. The sloped floor surface is captured by the slope angle, denoted by ϕ. We denote the walking activity pattern set $\mathcal{A}_N = \{a_1, a_2, \cdots, a_N\}$, where a_i, $i = 1, \ldots, N$, represents the ith walking pattern and N is the total number of walking patterns. The walking activity pattern refers to continuous walking gaits with subjects' self-selected speeds on level or sloped floors. Turning is not considered as a separate walking activity pattern in this study and instead, turning angle is part of the kinematics variables that will be estimated in real time.

As shown in Fig. 2(a), the human walker wore a single IMU at the shank location. We chose this IMU location because the previous study in [9] confirmed that it gave high sensitivity for detecting walking gaits. The joint angles of the human lower- and upper-limb in the sagittal plane are considered and illustrated as shown in Fig. 2(a). A total of 12 joint angles from lower- and upper-limbs are defined and introduced in this study, namely, left- and right-side shoulder, elbow, wrist angles, denoted by $\boldsymbol{\theta}_u = \{\theta^i_{\text{shoulder}}, \theta^i_{\text{elbow}}, \theta^i_{\text{wrist}}\}$, and hip, knee, and ankle angles, denoted by $\boldsymbol{\theta}_l = \{\theta^i_{\text{hip}}, \theta^i_{\text{knee}}, \theta^i_{\text{ankle}}\}$, in the sagittal plane, $i = l, r$ for left- and right-limb. Fig. 2(b) illustrates the schematic of the human turning angle, denoted by ψ, which is defined as the angle between the walker's facing direction and the X-axis of the global frame. In experiments, the subjects were asked to start at the same location with a same facing direction to ensure left/right symmetry and repeatability. For simplicity, we define the X-axis direction as the initial facing direction such that the turning angle is around zero at the beginning of each trial.

In walking gait, one stride period is defined as the time duration between consecutive heel strikes (i.e., touchdowns) of the same foot. We introduce the phase variable, denoted by s, to represent the normalized gait progression. The values of the phase variable s at the current and next foot heel strikes are $s = 0$ and 100%, respectively. The walking gait progression is represented as a continuous function of s that smoothly varies from 0 to 100% over the course of a single stride. With the above configuration, we consider the following problem.

Problem Statement: For given walking activity set $\mathcal{A}_N$, the goal of this study is to detect the walking activity a_k, $1 \leq k \leq N$, and estimate the upper- and lower-limb joint angles ($\boldsymbol{\theta}_u$ and $\boldsymbol{\theta}_l$), turning angle ψ, slope angle ϕ and phase variable s in real time by only using a single wearable IMU.

In this study, we mainly focus on five types of human walking activity patterns, that is, $N = 5$. These activities include: straight walking on the level ground (a_1), walking up on the slope (a_2), body turning (include turning in place and turning while walking) (a_3), walking transverse the slope (a_4) and walking down the slope (a_5); see illustrative examples in Fig. 1. We chose these walking activities primarily because they are common in construction and the methodologies developed here are extendable to other walking activities.

III. Experiments and Data Collection

In this section, we first present the experimental configurations and protocols and then discuss data collection.

A. Experimental Setup and Protocols

Fig. 1 shows the overview of the experimental setups. A laboratory setup was created to mimick a construction work environment for human subjects walking on the level and sloped surfaces. A wooden slope structure with glued anti-skid tapes was designed as a roof structure and the slope angle can be adjusted up to 40 deg. In training experiments, a level floor surface (i.e., $\phi = 0$ deg) and a set of slope angles (i.e., $\phi = 5, 10, 15$ deg) were selected to represent common roof slopes encountered in construction. These angles span a

range of biomechanical challenges, from mild to steep inclines, and therefore, experiments would be used to comprehensively evaluate the system's performance. Intermediate angles (i.e., ϕ = 8 and 12 deg) were included in experiments to test the model's generalization capability.

To measure the human kinematics and motion, a small-size IMU (from LP-RESEARCH Inc.) was attached to the right shank of the subject; see Fig. 2(a). The Bluetooth IMU measurements include 4 quaternions readings for attitude angles, 3-axial gyroscope rates and 3-axial linear accelerations. The gyroscope offers a measurement range of up to $\pm$2000 deg/s with a 16-bit resolution, while the accelerometer supports measurements of up to $\pm$16 g, also with a 16-bit resolution. The orientation capabilities include roll ($\pm$180 deg), pitch ($\pm$90 deg), and yaw ($\pm$180 deg), with a resolution of finer than 0.01 deg and an accuracy of less than 0.5 deg in static conditions and 2 deg root mean square (RMS) in dynamic conditions. The IMU was carefully placed on the same location of the right shank segment (around 20 cm above the ankle joint) before each trial and the orientation was the same across subjects. The IMU captured the dynamic features of turning motions, which exhibited consistent temporal patterns across both left and right turns. By taking advantages of these shared patterns, the framework was able to robustly classify turning motions as a single class.

To record reference motion data, a motion capture system (8 Vantage cameras, Vicon Motion Systems Ltd.) was used to collect marker positions. The Vicon full-body plugin gait marker set was used and the optical markers were placed on subjects' lower and upper limbs, trunk and head to represent full-body motion. The ground truths for joint angles ($\boldsymbol{\theta}_u$ and $\boldsymbol{\theta}_l$), turning angle ψ, and gait phase s were calculated using custom algorithms in MATLAB software (Version R2020a, MathWorks Inc.) and the optical marker positions. The slope angles were carefully measured and recorded before each experimental trial. These ground truth data were used for model training, validation, and real-time performance evaluation.

Eight healthy subjects (six males and two females, age: 30$\pm$3 years, weight: 73.3$\pm$6.5 kg, height: 172.0$\pm$6.7 cm) were recruited for experiments. The subjects were capable of walking on level and sloped surfaces and were reported without any orthopedic disease history. The subjects were instructed to use their normal gaits and self-selected walking speeds. An informed consent form was signed by all the subjects, and the Institutional Review Board at Rutgers University approved the testing protocols.

The experimental design was divided into two main phases: Training data collection and real-time validation and evaluation. Each phase consisted of multiple sessions that were designed to capture a variety of walking patterns under different conditions. The training data collection phase comprised three sessions, focusing on walking activity patterns on level floor and slopes with varying angles.

- Session E1 (Level ground walking): Subjects were instructed to walk straight back and forth on level ground for four minutes. This session aimed to establish a baseline for walking patterns on level floors.
- Session E2 (Turning while walking): Participants followed the marked trajectories with small and large turning radii on level ground, making turns while walking for four minutes. This session evaluated the subjects' turning behavior on flat surfaces.
- Session E3 (Slope walking): Three slope angles (ϕ = 5, 10, 15 deg) were tested. As shown in Fig. 1(a), for each slope, subjects started on the slope, walked up the slope, made a sharp turn, traversed across the slope, made another sharp turn, walked down the slope, turned, and traversed back to the starting point in a clockwise direction. This sequence was repeated for four minutes, followed by trials in the reverse (counter-clockwise) direction for the same amount of time to ensure left and right turns are equally represented, with a two-minute break between trials. This session assessed walking patterns on slopes, incorporating turns and transverse movements.

The real-time validation and evaluation experiments consisted of two sessions, aiming at testing the robustness of the algorithms and evaluating the algorithm's performance on untrained slopes.

- Session E4 (Slope walking with marked trajectory): Subjects followed a marked trajectory on the floor and slope in a clockwise direction for four minutes for each slope angle set, and then reversed (counter-clockwise) the walking direction for another trial. Two turning radii were considered, as shown in Fig. 1(b).
- Session E5 (Untrained slope angles): This session aimed to evaluate the algorithm's adaptability to new conditions by testing its performance on slopes not encountered during the training phase. The experimental platform was adjusted to inclines of 8 and 12 deg, i.e., ϕ = 8, 12 deg. Subjects replicated the tasks from Session E4 under these two slope angles. To demonstrate the setup for assessing continuous performance on untrained slopes, Fig. 1(c) illustrates the experimental platform. Participants first ascended an 8-deg slope, turned 90 deg, and then descended a 12-deg slope, followed by a trial in the reverse direction. This session aimed to test and evaluate the algorithm with slopes and turning angles not encountered during the training phase in real time.

B. Data Processing

Fig. 3 shows the system design architecture for the real-time activity detection and posture estimation. During data collection, motion data were collected at a sampling frequency of 100 Hz and processed using Vicon Nexus software for accurate ground truth validation. IMU measurements were wirelessly transmitted to the Raspberry Pi at a frequency of 100 Hz via Bluetooth. The Raspberry Pi received and synchronized data from up to seven IMUs. The processed IMU data was then transmitted to a portable embedded computer (Intel NUC7i7DNK, Intel Corp.) via a serial communication connection. A Python multiprocessing pipeline synchronized both the IMU and motion data during offline collection and real-time testing. The IMU and motion capture data were

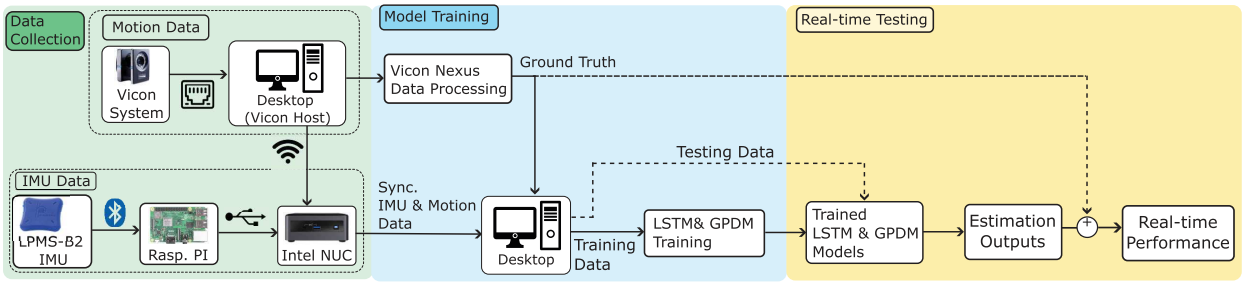

Fig. 3. Data streaming overview: During data collection, we collected and synchronized the motion data with IMU signals on a portable Intel NUC computer. The training data were processed and input to the neural networks to build the models on a PC. Finally, The system runs in real-time with the training models on the same PC and output estimation results. The motion capture data serves as ground truth during model training and real-time testing.

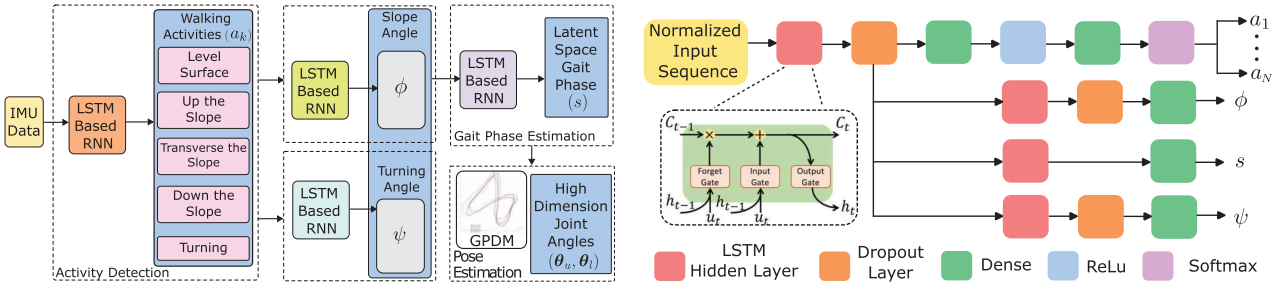

Fig. 4. (a) Flowchart of the human walk gait detection process, illustrating the stages from activity detection to slope and turning angle estimation, gait phase detection, and pose estimation. (b) Detailed architecture of the LSTM-based RNN neural network for predicting walking activities, slope angle, gait phase, and turning angle.

further pre-processed using customized MATLAB scripts on a desktop computer (Dell XPS-8953, Dell Inc.), which was equipped with an Intel i7-8700 CPU, Nvidia 1030 GPU, Samsung 860 EVO SSD, and 16 GB RAM. Walking activities were labeled according to distinct patterns. Stride information, including heel strike time, stride length, and walking speeds, was extracted from the motion capture data.

The beginning and end of each stride were defined using the location of heel markers. IMU data were concatenated for the same activities, and the corresponding sections were extracted based on the motion capture data. For training purposes, IMU data were reshaped, and 60 consecutive frames were combined into a single frame of data. The IMU sequence data were normalized using the mean and standard deviation of the dataset, which was then used as input for the model. In the testing phase, 59 past frames and one current frame were combined to form the input to the activity detection and posture estimation model. The same mean and standard deviation were used to standardize and normalize the real-time IMU data, i.e., the IMU sequence was subtracted by the mean and divided by the standard deviation of the training data. Each experimental trial lasted approximately 5 minutes. The dataset was evenly distributed among different gait activities to ensure balanced model training and evaluation. For experiments E1 to E3, a total of $3,200,000$ data points were collected and an 80-20 split of the dataset was used for LSTM-GPDM training and model development.

The pre-trained models and neural network parameters were stored on the same desktop computer, which was also used for real-time testing. For real-time testing and evaluation purpose, the IMU sequence data were streamed into the learned model, enabling the detection of the subject's walking activities and estimation of human posture. In a real-time application, foot strikes were detected by inspecting the sudden drop in the gait phase variable and the linear acceleration data. When each walking cycle ended and a foot strike was detected, the gait phase variable s was reset to the beginning of the stride (i.e., $s = 0$). For real-time performance evaluation experiments E4 and E5, a total of about $800,000$ data points were used and they were not for any model training purposes.

IV. Learning-Based Gait Detection and Pose Estimation

A. Design Overview

Fig. 4(a) illustrates the design flowchart of the walking activity detection and pose estimation scheme. The design contains five modules: walking activity a_k detection, slope angle ϕ and turning angle ψ estimation, gait phase s and full-body posture (joint angles) estimations for any given time. An LSTM-based classification and regression model is used to identify the walking activity $a_k \in \mathcal{A}_N$ (for $N = 5$ in the study). The estimated slope angle ϕ and the turning angle ψ are also obtained for identified activity by using the LSTMs. The gait phase variable $s \in [0, 1]$ are estimated using the LSTM-based RNN. Finally, the full-body posture (i.e., joint angles $\boldsymbol{\theta}_u$ and $\boldsymbol{\theta}_l$) estimation scheme is obtained using the GPDM model. In the following, we describe each of these modules in details.

B. RNN-Based Activity Detection and Gait Estimation

Fig. 4(b) shows the schematic of the four-layer of the LSTM-based design. The module detects the walking activity a_k for N-activity classification (i.e., selection of $a_k \in \mathcal{A}_N$), slope angle ϕ, gait phase s, and turning angle ψ estimation. The

LSTM is an RNN architecture to learn sequential information using memory cells that stores and outputs information to capture the temporal relationships. Using a single IMU for gait detection presents several challenges, primarily due to the limited scope of measurements that it provides. The LSTM network effectively compensates for this limitation by exploiting the temporal correlations in the IMU data.

LSTM networks are chosen for their ability to model long-term temporal dependencies in sequential data, such as gait cycles and transitions. Their internal gating mechanisms allow the model to retain information over time and to capture complex temporal patterns and dependencies in human gait data. By using LSTM networks, we extract meaningful patterns from the IMU data, leading to robust and reliable estimations of gait and posture. As shown in Fig. 4(b), the information update is through various gates and the relationships among the input gate, forget gate and output gates [36]. The first stage of the method includes the LSTM-based classification and regression models. The LSTM model is built on the training data collected from IMUs and motion capture system.

For training purposes, the raw IMU data were collected and labeled for $\mathcal{A}_N$ with five walking patterns and different slope angles (i.e., ϕ = 0, 5, 10, and 15 deg). The raw IMU data consisted of 10 channels (3-axial gyroscope rates, 3-axial linear accelerations, and 4 quaternions) directly from a single IMU that was manually labeled using ground truth data from the motion capture system. The IMU data were scaled to fit between zero and one and reshaped to three-dimensional inputs (i.e., samples, time steps, features) for the LSTM models. The reshaped data was split into training and validation datasets using an 80-20 split. This split was used to evaluate the LSTM's performance during development and ensured its ability to generalize to unseen data within the training process. For real-time testing and final evaluation, the model was evaluated on completely separate trials, which were not included in the training dataset.

The activity classification model consists of a single LSTM hidden layer with 50 neurons. To mitigate overfitting, the output of the LSTM layer is passed through a `Dropout` layer, which randomly drops 20% of the units during training. The outputs from the `Dropout` layer are then fed into a fully connected layer with 50 neurons using a rectified linear unit (`ReLU`) activation function. The `ReLU` activation function is selected to handle large-scale data efficiently and address the vanishing gradient issue to ensure stable training of the model. Finally, the fully connected hidden layer connects to a `Softmax` activation function, which converts class scores into probabilities to identify the activity with the highest likelihood.

The slope angle ϕ and turning angle ψ estimation modules are implemented using a two-layer stacked LSTM network. The first LSTM layer contains 64 neurons, followed by a `Dropout` (20%) layer. The output of the first LSTM is passed to the second LSTM layer, which is followed by another `Dropout` (20%) layer to further mitigate overfitting. The final output layers of these modules generate regression outputs for the slope and turning angles. It is important to note that the gait phase variable s is assumed to increase monotonically within each stride. This implies that it increases consistently from the beginning to the end of each stride. This observation is crucial for the accurate estimation of s using the LSTM-based RNN model. To estimate the s values, we develop another LSTM-based RNN and the lower layer in Fig. 4(b) shows the corresponding network architecture. The gait phase estimation model contains a two-stacked LSTM-based networks with one `Dropout` (20%) layer between them, while both LSTM hidden layers have 32 neurons.

For all models, appropriate task-specific loss functions were applied. The activity classification model employed categorical cross-entropy loss function to accurately predict discrete activity labels, while the mean squared error (MSE) was used for regression tasks, including estimating joint angles, slope angles, turning angles, and gait phases. The model fit was assessed by examining the loss and accuracy curves during training. All modules were trained simultaneously in a multi-task learning framework, with the Adam optimizer employed to update the weights efficiently. This simultaneous training allowed the shared LSTM to learn generalized temporal features, while the task-specific layers refined outputs for their respective objectives. Extensive ablation studies were conducted during model development to evaluate the impact of shared LSTM structures, task-specific output layers, and loss function choices for the final configuration that balanced accuracy and robustness effectively.

C. GPDM Model and Full-Body Pose Estimation

The GPDM framework is selected for its ability to represent human motion in a low-dimensional latent space with physical interpretability. Unlike deep learning models that often require additional analysis to interpret learned features, GPDM naturally provides a meaningful manifold reflecting biomechanical relationships. Additionally, the low inference cost of GPDM makes it particularly suitable for real-time applications.

The cyclic walking gaits in the high-dimensional joint angle space are represented in low-dimensional latent space as learned closed-shape manifolds. We denote the full-body joint angle as $\boldsymbol{\theta} \in \mathbb{R}^D$ and the latent state variable as $\boldsymbol{x} \in \mathbb{R}^d$, where d and D ($d \ll D$) are the dimensions of the latent space and the joint angle space, respectively. For each type of the walking activity a_i, $i = 1, \cdots, N$, and slope angle ϕ, the latent dynamics for human motion are formulated as

$$\mathcal{M}_i(\phi): \begin{cases} \dfrac{d\boldsymbol{x}_i}{ds} = \boldsymbol{f}_i(\boldsymbol{x}_i, \boldsymbol{\alpha}_i, \boldsymbol{u}_i) + \boldsymbol{w}_{pi}, \\ \boldsymbol{\theta}_i = \boldsymbol{g}_i(\boldsymbol{x}_i, \boldsymbol{\beta}_i, \boldsymbol{u}_i) + \boldsymbol{w}_{oi} \end{cases} \tag{1}$$

where $\boldsymbol{x}_i = \boldsymbol{x}_i(s)$, $\boldsymbol{\theta} = \boldsymbol{\theta}_i(s)$, and $\boldsymbol{u}_i = \boldsymbol{u}_i(s)$ are latent state, joint angles and IMU measurements at gait phase variable s, respectively. $\boldsymbol{\alpha}_i$ and $\boldsymbol{\beta}_i$ are GP parameters and obtained from learning process, $\boldsymbol{w}_{pi}$ and $\boldsymbol{w}_{oi}$ are zero mean model noises for the state dynamics and output models, respectively. In the training phase, the IMU data set $\boldsymbol{U}_i = \{\boldsymbol{u}_i\}^M$ and joint angle set $\boldsymbol{Y}_i = \{\boldsymbol{\theta}_i\}^M$ (with M data points) are obtained for walking on the surface with slope angle ϕ. We then estimate the mappings $\boldsymbol{f}_i(\cdot)$ and $\boldsymbol{g}_i(\cdot)$ in (1) by identifying parameters $\boldsymbol{\alpha}_i$ and $\boldsymbol{\beta}_i$ through minimizing the posterior probability

$$\mathcal{L}_i = -\ln p(\boldsymbol{X}_i, \boldsymbol{\alpha}_i, \boldsymbol{\beta}_i | \boldsymbol{Y}_i, \boldsymbol{U}_i, \hat{\boldsymbol{X}}_i), \tag{2}$$

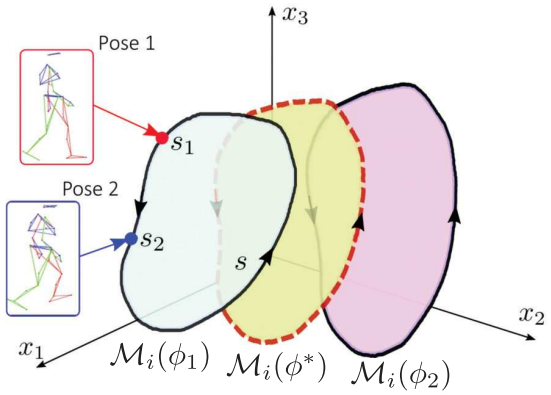

Fig. 5. Schematic of the learned manifolds $\mathcal{M}_i(\phi_1)$ and $\mathcal{M}_i(\phi_2)$ that are obtained at slope angles ϕ_1 and ϕ_2 for activity a_i. Manifold $\mathcal{M}_i(\phi^*)$ is an estimated from interpolation from $\mathcal{M}_i(\phi_1)$ and $\mathcal{M}_i(\phi_2)$.

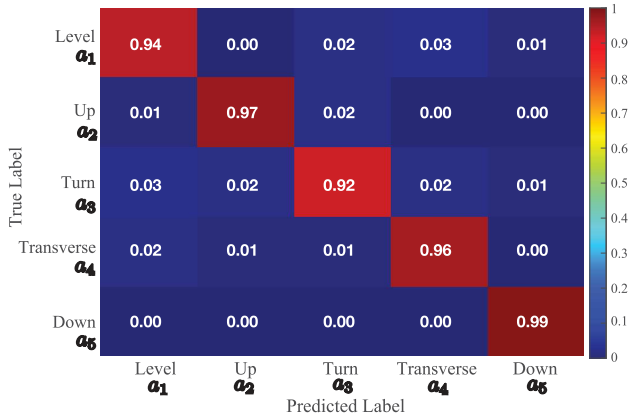

Fig. 6. Confusion matrix for classification of five different activities.

where $\hat{\boldsymbol{X}}_i = \{\hat{\boldsymbol{x}}_i\}^M$ is used to initialize $\boldsymbol{X}$ in the optimization process (i.e., label of $\boldsymbol{X}$), and probability $p(\boldsymbol{X}_i, \boldsymbol{\alpha}_i, \boldsymbol{\beta}_i | \boldsymbol{Y}_i, \boldsymbol{U}_i, \hat{\boldsymbol{X}}_i) \propto p(\boldsymbol{Y}_i | \boldsymbol{X}_i, \boldsymbol{\beta}_i) p(\boldsymbol{X}_i | \boldsymbol{U}_i, \boldsymbol{\alpha}_i) p(\boldsymbol{X}_i | \hat{\boldsymbol{X}}_i) p(\boldsymbol{\alpha}_i) p(\boldsymbol{\beta}_i)$.

It is known that nearby points in the joint angle space are likely located close together in the latent space [37]. Therefore, level curves associated with the same activity share the same topological shapes in the latent space with small variations. This dimensionality reduction and latent representation allow us to efficiently model complex human motions in a compact form, which is crucial for generalizing across different walking activities and slope angles. Fig. 5 illustrates the above-discussed learned motion manifold concept. Manifolds $\mathcal{M}_i(\phi_1)$ and $\mathcal{M}_i(\phi_2)$ are obtained respectively by training the GPDM models with datasets at slope angles ϕ_1 and ϕ_2 for a specific activity (a_i). Poses 1 and 2 represent specific postures on the manifold at the corresponding phase variables s_1 and s_2, respectively. The phase-based interpolation ensures a smooth transition between manifolds and enables accurate prediction of kinematic variables. To estimate the manifold $\mathcal{M}_i(\phi^*)$ at a given slope angle ϕ^*, we use interpolation between $\mathcal{M}_i(\phi_1)$ and $\mathcal{M}_i(\phi_2)$, as illustrated in Fig. 5. The slope angle ϕ^* is represented as $\phi^* = \gamma\phi_1 + (1-\gamma)\phi_2$, where $0 \leq \gamma \leq 1$ is a weight factor that determines the contribution of ϕ_1 and ϕ_2 to the interpolation. This formulation ensures the interpolation is proportional to the proximity of ϕ^* to the learned manifolds. It also enables the system to generalize its joint angle estimations to novel slope angles not explicitly included in the training data.

The GPDM captures the inherent structure and dynamics of human motion in a low-dimensional latent space, offering several key advantages for pose estimation. GPDM reduces the dimensionality of the joint angle space, making real-time pose estimation computationally feasible. As a probabilistic model, GPDM captures the uncertainty in the mapping between the latent space and the joint angle space, enabling robust pose estimation in the presence of noise and variability. Comparing with other techniques in [33], the model in (1) is progressed with phase variable s, rather than time t. The advantage of this treatment is from the observation that the manifold $\mathcal{M}_i(\phi)$ is a closed-curve in latent space, effectively capturing the periodic nature of human walking motion. This parameterization facilitates the estimation of poses at different gait phases. Once GPDM $\mathcal{M}_i(\phi^*)$ is obtained from activity a_i with slope angle ϕ^*, the latent state $\boldsymbol{x}_i(s)$ is predicted using variable s and the learned latent dynamics, and the corresponding joint angles $\boldsymbol{\theta}_i(s)$ are estimated using the output equation of (1).

V. Experimental Results

In this section, we present the real-time performance evaluation results from experiments E4 and E5. We first present the real-time walking activity detection results. Fig. 6 shows the confusion matrix for the real-time activity classification from all subjects and trials. The results confirm that the model performs exceptionally well in classifying upslope, downslope, and transverse walking, with accuracies around 96%. The model occasionally mis-classified the the level walking with transverse walking while turning, which can be attributed to the subtle differences in the motion patterns of these activities. The overall accuracy of the activity classification model remains high, indicating its effectiveness in identifying different walking conditions.

Fig. 7 shows a comprehensive analysis of the real-time prediction performance by comparing the actual gait activity, slope angle ϕ, and turning angle ψ with the model's predictions for a 15-deg sloped walking trial. The top plot demonstrates the model's ability to accurately predict gait activities a_i, with only occasional mis-classifications. The middle and bottom plots illustrate the performance of the slope and turning angles estimation models, respectively. The slope angle predictions closely match the actual values, with the relatively large errors occurring during downslope walking. The turning angle predictions also exhibit a strong correspondence with the actual values, capturing the dynamic changes in the subject's orientation throughout the trial. Slight deviations are observed during transitions between different walking activities, indicating the challenges in estimating turning angles during these dynamic phases. The zoom-in plot in Fig. 7 provides the gait phase variable s estimation for five complete gait cycles. A representative length of a gait cycle is also marked, as s increases from 0 to 100%. The model's estimates closely follow the ground truth values and this demonstrates its ability to capture the temporal evolution of the gait phase.

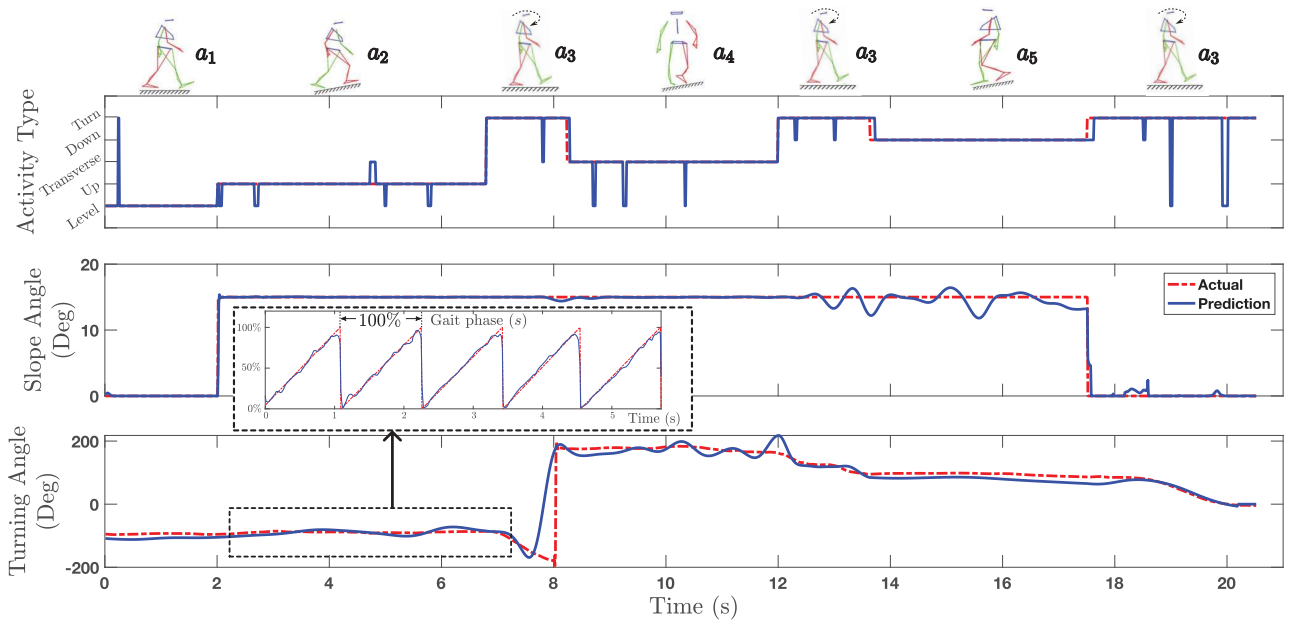

Fig. 7. Real-time gait activity detection, slope angle ϕ estimation, and turning angle ψ prediction results during one complete 15-deg sloped walking trial. Predicted values (blue solid lines) versus the actual values (red dashed lines). The results demonstrate the model's capacity to predict walking activities with infrequent misclassifications.

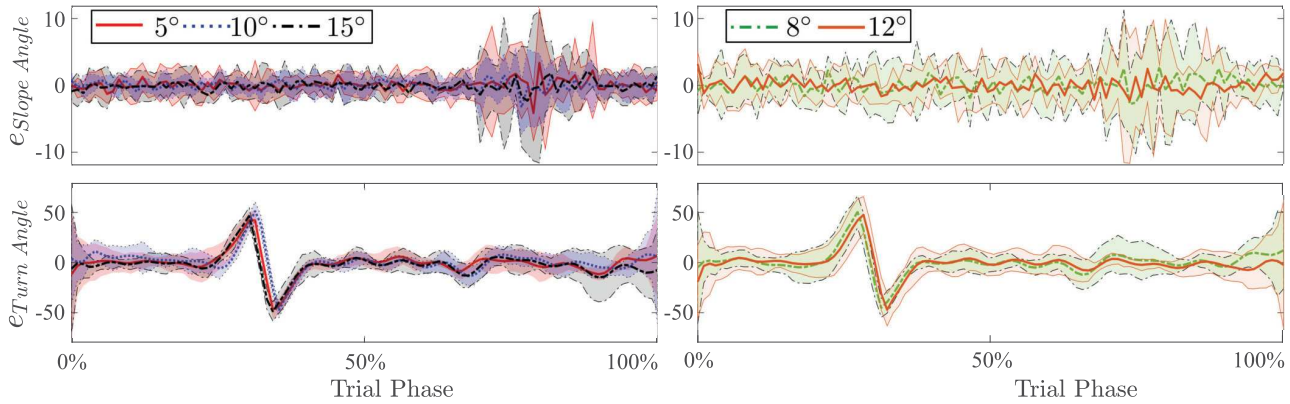

Fig. 8. Real-time slope angle ϕ and turning angle ψ prediction results for the proposed method. The x-axis data is normalized with respect to the running time of each trial. The left column shows the prediction errors for trained slope angles $\phi = 5, 10, 15$ deg, while the right column presents the results for untrained slope angles, i.e., $\phi = 8$ and 12 deg. The prediction errors are normalized to the trial time length. The top and bottom rows correspond to the slope angle ϕ and turning angle ψ predictions, respectively. The solid lines represent the mean error profiles, and the shaded areas indicate the standard deviation bands.

Fig. 8 shows multi-subject results for the slope and turning angles estimation errors over 30-s experiment trials. The time is normalized to the trial duration for consistent comparison across different walking conditions. The left column of the figure focuses on the prediction errors for trained slope angles ($\phi = 5, 10$, and 15 deg), while the right column presents the results for untrained slope angles ($\phi = 8$ and 12 deg). For the trained slope angles, the system demonstrates higher accuracy throughout the gait cycle. The small standard deviations indicate consistent performance across different gait phases and subjects. On the other hand, the results for the untrained slope angles provide insights into the system's generalization capability. Despite not being explicitly trained on slopes of 8 and 12 deg, the prediction algorithm maintains a reliable performance.

Table I lists the root mean square error (RMSE) results for slope angle, turning angle, and gait phase estimation across different walking activities. The proposed algorithm and design demonstrate high accuracy, with RMSE values ranging from 1.19 to 2.47 deg for slope angle estimation, indicating its ability to precisely estimate the inclination of the walking floor. Similarly, the RMSE values for turning angle estimation range from 13.85 to 18.23 deg, showcasing the system's capability to accurately capture the changes in body

TABLE I
RMSEs FOR SLOPE ANGLE ϕ, TURNING ANGLE ψ, AND GAIT PHASE s ESTIMATION FROM DIFFERENT WALKING ACTIVITIES

Slope ϕ (deg)	Slope angle ψ estimation (deg)	Turning angle ψ estimation (deg)	Gait phase s estimation
5	1.19 ± 0.10	13.85 ± 3.88	$5.44 \pm 0.86\%$
10	1.18 ± 0.11	15.24 ± 2.47	$5.94 \pm 0.87\%$
15	1.59 ± 0.23	18.23 ± 4.38	$6.42 \pm 1.62\%$
8	2.45 ± 0.34	16.80 ± 3.08	$6.08 \pm 1.71\%$
12	2.47 ± 0.26	15.68 ± 4.31	$6.13 \pm 1.24\%$

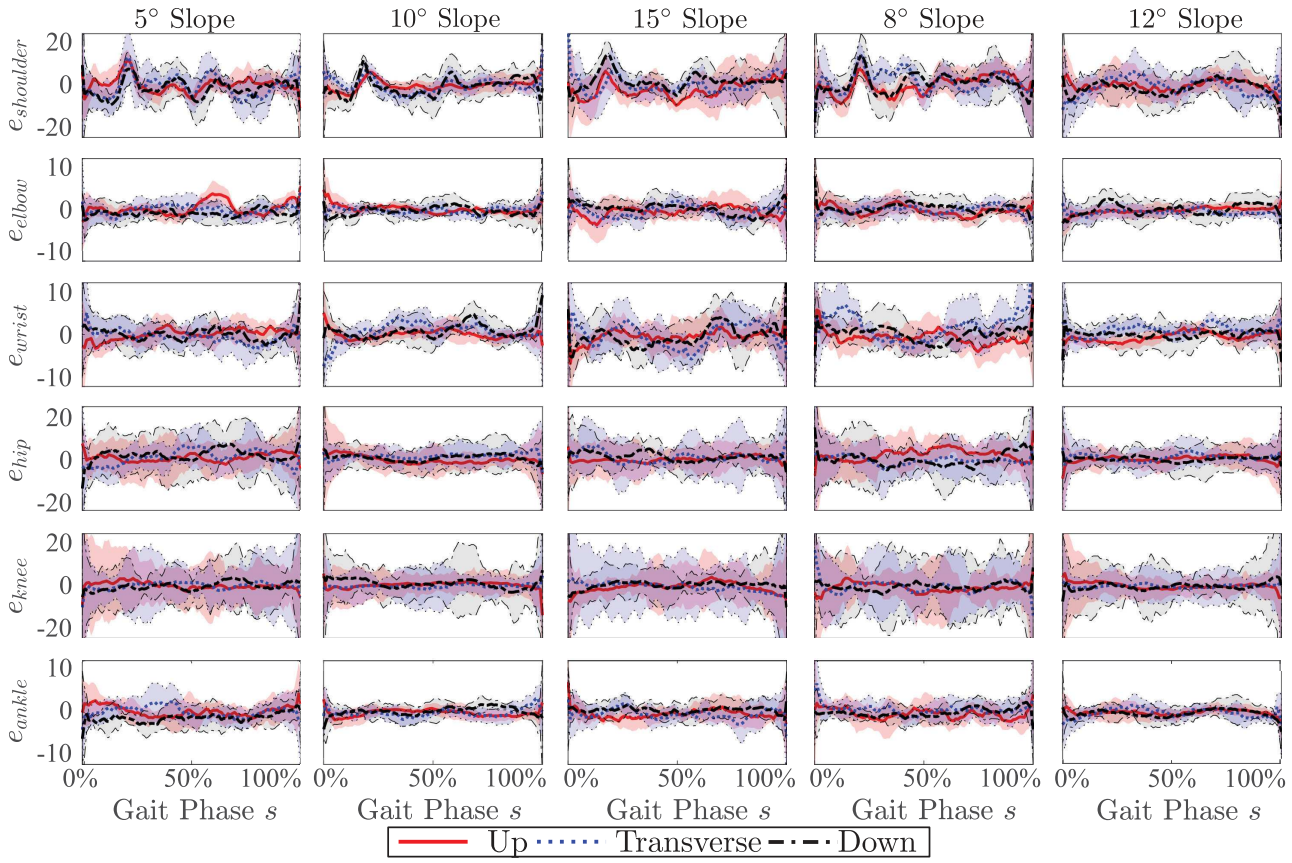

Fig. 9. Comparison of the joint angle error profiles for variable slope angles ($\phi = 5, 10, 15, 8, 12$ deg) during different activities $\mathcal{A}_5$ among all subjects. The plot show the error profiles (i.e., mean $\pm$ std) in the order of right shoulder (e_{shoulder}), elbow (e_{elbow}), wrist (e_{wrist}), hip (e_{hip}), knee (e_{knee}), and ankle (e_{ankle}). The thick curves are the mean error profiles, while the shaded ares show the one standard deviation around the mean values of all subjects.

orientation during walking gait. The low RMSEs for gait phase estimation, ranging from 5.44 to 6.42%, highlight the system's proficiency in tracking the progression of the gait cycle. These results underscore the overall effectiveness of the proposed approach in accurately estimating key gait parameters across various walking activities.

Fig. 9 shows the comparison of joint angle errors for different slope angles and walking activities. The figure focuses on the right-limb joint angles, namely, right shoulder, elbow, wrist, hip, knee and ankle angles. It is clear that the shoulder and knee joint angle estimates exhibit slightly larger errors compared to that of the hip joint angle, particularly during the stance phase ($0 \leq s \leq 50\%$). This may be attributed to the greater range of motion and variability in the shoulder and knee joints during walking. Despite these variations, the overall joint angle estimation accuracy remains high and this demonstrates the system's ability to capture the dynamics of lower limb movements during gait on uneven floor surfaces.

Table II lists of the RMSEs of the joint angle estimation for all activities on sloped floors. Due to the symmetric motion patterns between the left- and right-limb in walking gait, the listed RMSEs were computed by combining the corresponding limb joint angles. The results demonstrate varying levels of accuracy across joints, activities, and inclines. The elbow and wrist joints demonstrate the lowest RMSE values, ranging from approximately 1.17 to 4.25 deg, indicating high estimation accuracy. In contrast, the knee joint consistently exhibits the highest RMSE values among all joints, peaking at 17.09 ± 1.10 deg for transverse movement on the 15-deg floor surface. Hip and shoulder joints show moderate errors, typically between 3 and 9 deg. The estimation accuracy on the flat surface is generally higher than that on the sloped surface, with lower RMSE values across all joints for straight walking. The data also suggests that estimation accuracy tend to decrease with increasing slope angle, particularly for lower-limb joints, likely due to the complex biomechanics involved in navigating steep inclines.

Table III lists the computational and latency results to show the real-time performance of the proposed system on the desktop computer mentioned in Section III-B. The average processing time per frame is 18.1 ms and the average latency is 21.6 ms. These results demonstrate the system's capability to process and respond to incoming data quickly. The breakdown of computation times for different stages of the pipeline reveals that the pose estimation stage was the most time-consuming, requiring 9.6 ms per frame. This highlights the computational complexity associated with estimating full-body postures. Nevertheless, the overall computation time remains within acceptable limits, allowing for real-time operation of the system. These performance metrics underscore the efficiency and practicality of the proposed approach for real-time activity detection and pose estimation in industrial applications.

TABLE II
RMSEs OF 12 JOINT ANGLES FOR ALL SUBJECTS DURING DIFFERENT ACTIVITIES

Slope Angle ϕ (deg)	Activity	θ_{Shoulder} (deg)	θ_{Elbow} (deg)	θ_{Wrist} (deg)	θ_{Hip} (deg)	θ_{Knee} (deg)	θ_{Ankle} (deg)
5	Up	5.89 ± 0.60	2.00 ± 0.13	2.78 ± 0.26	8.45 ± 0.93	11.08 ± 1.57	4.21 ± 0.50
	Transverse	7.87 ± 0.54	2.11 ± 0.17	3.49 ± 0.27	8.99 ± 0.44	10.84 ± 1.77	4.72 ± 0.63
	Down	7.62 ± 0.71	1.92 ± 0.08	3.21 ± 0.34	9.87 ± 0.59	11.14 ± 1.10	5.08 ± 1.02
10	Up	3.63 ± 0.27	1.56 ± 0.23	1.85 ± 0.19	6.86 ± 0.65	9.63 ± 1.47	5.48 ± 0.28
	Transverse	4.32 ± 0.33	1.35 ± 0.14	2.83 ± 0.21	5.56 ± 0.44	8.39 ± 0.61	6.52 ± 0.45
	Down	6.68 ± 0.56	2.14 ± 0.22	2.78 ± 0.18	8.13 ± 0.46	13.95 ± 1.00	7.59 ± 1.00
15	Up	6.94 ± 0.49	2.66 ± 0.20	3.71 ± 0.33	6.53 ± 0.54	13.11 ± 0.88	6.14 ± 0.71
	Transverse	6.58 ± 0.54	2.44 ± 0.19	3.93 ± 0.32	9.01 ± 0.93	17.09 ± 1.10	7.96 ± 0.82
	Down	8.26 ± 0.63	2.11 ± 0.16	4.25 ± 0.25	8.98 ± 0.81	12.71 ± 1.52	8.04 ± 0.52
8	Up	6.54 ± 0.47	2.24 ± 0.15	3.44 ± 0.31	8.89 ± 0.53	12.45 ± 0.95	3.75 ± 0.97
	Transverse	7.81 ± 0.77	1.91 ± 0.21	3.77 ± 0.33	8.65 ± 0.48	11.67 ± 1.27	4.32 ± 1.00
	Down	8.37 ± 0.87	2.36 ± 0.21	3.06 ± 0.19	9.57 ± 0.58	12.87 ± 0.81	5.51 ± 0.51
12	Up	3.57 ± 0.23	1.46 ± 0.17	1.92 ± 0.19	5.76 ± 0.65	9.04 ± 1.51	5.77 ± 0.33
	Transverse	4.19 ± 0.29	1.53 ± 0.14	2.46 ± 0.19	6.27 ± 0.58	9.16 ± 1.01	7.22 ± 0.51
	Down	6.91 ± 0.37	2.36 ± 0.12	2.78 ± 0.19	8.96 ± 0.25	13.61 ± 1.10	7.25 ± 0.48
0 (level)	Straight Walk	3.16 ± 0.31	1.17 ± 0.23	2.89 ± 0.33	5.37 ± 0.97	10.16 ± 1.58	3.61 ± 0.47
	Turn & Walk	4.53 ± 0.45	1.52 ± 0.30	3.22 ± 0.40	7.03 ± 1.21	12.31 ± 1.80	5.33 ± 0.68

TABLE III
AVERAGE COMPUTATION AND LATENCY OF THE PROPOSED SYSTEM

Processing time per frame (ms)	Estimation latency (ms)				
	$\mathcal{A}_N$	ϕ	ψ	s	$\boldsymbol{\theta}$
18.1	2.2	2.7	3.1	3.5	9.2

TABLE IV
PERFORMANCE AND SENSOR COMPARISON BETWEEN THE PROPOSED METHOD AND OTHER APPROACHES (ENC., FSR AND FP STAND FOR ENCODER, FORCE SENSITIVE RESISTOR, AND FORCE PLATE, RESPECTIVELY)

Algorithm / RMSE	This work	[17]	[22]	[24]	[38]	[39]
Slope Angle (deg)	2.1	N/A	1.5	1.25	1.7	1.3
Gait Phase	10.8%	5.04%	N/A	N/A	N/A	N/A
Joint Angle (deg)	8.7	N/A	N/A	N/A	N/A	N/A
Used sensors	IMU	IMU, Enc., FSR	IMU, Enc., FSR	IMU, EMG, GON	IMU, GON, FP	IMU, Enc., EMG

VI. DISCUSSIONS

In this work, we presented a machine learning-based approach for walking activity classification, slope angle and human turning angle estimation, and human joint angle prediction using a single IMU. The choice of LSTMs was motivated by their ability to effectively capture the sequential and temporal dependencies in gait dataset, while the spatial relationships of joint positions are handled by the GPDM. The hybrid framework integrates both spatial and temporal analysis for robust activity recognition and posture estimation. To further validate the system design, we extended our evaluation to an alternative data set in [38]. The data set contains sensor data from 3 IMUs and 3 electrogoniometers, and 13 static-slope and 4 dynamic-slope trials. The static-slope trials involves walking on fixed slopes at varying walking speeds and the dynamic-slope trials involves walking on variable slopes at fixed walking speeds. By assessing the proposed algorithm's performance on this diverse data set, we aim to affirm its adaptability to different walking conditions and sensor configurations.

We implemented the proposed algorithm using only the IMU data mounted on the shank, as described in [38], and conducted performance evaluation. The outputs of the proposed model included slope angle, gait phase, and lower-limb joint angles (hip, knee, and ankle angles in the sagittal plane). Table IV lists the comparison results with other related works, as well as the sensor types. For slope angle estimation, the proposed algorithm achieved an RMSE of 2.1 deg, which is comparable to 1.5 deg in [22], 1.25 deg in [24], 1.7 deg in [38], and 1.3 deg in [39]. This demonstrates the competitiveness of the proposed approach with the established methods. Despite of using a single IMU, the gait phase estimation of the proposed method also exhibits a comparable error (10.8%) with that in [17] (5.04%). Furthermore, the proposed algorithm demonstrated significant versatility by estimating three joint angles (hip, knee, and ankle) with an RMSE of 8.7 deg, a capability not provided by any of the other aforementioned works. This highlights the comprehensive gait analysis and posture estimation potential of the proposed approach.

The above comparative analysis with the other state-of-the-art methods highlights the competitiveness of the proposed approach, despite relying on only a single IMU. Notably, [17] used IMUs on the trunk and thighs, bilateral hip joint encoders, and heel force sensitive resistors. The work in [22] employed absolute knee joint encoders, shank and thigh-cuff 6-axis IMUs, and heel FSRs. Reference [24] unilaterally instrumented 11 EMG sensors, 3 GONs, and 4 IMUs. Three

6-axis IMUs, three two-degree-of-freedom GONs, and force plates were used in [38]. Reference [39] fused measurements from a hip joint encoder with the trunk and thigh IMUs, along with 8-channel EMG sensors. The authors also compared the results from the IMU and encoder with EMG measurements. The proposed system also achieved an average 21.6 ms latency due to the the multithreaded network design and sensor simplicity. In comparison, [17] and [40] reported 29 ms and 20 ms of real-time latencies, respectively. While incorporating additional sensors can potentially further improve the accuracy, the proposed approach showcases the potential of achieving comprehensive gait analysis with a streamlined sensor setup and comparable results with minimal sensor requirements.

The single-IMU design was chosen to ensure simplicity and practicality for real-time applications. The confusion matrix analysis in Fig. 6 highlights the model's high accuracy in classifying distinct activities such as upslope and downslope walking. However, misclassifications were observed between activities with subtle differences in IMU signal patterns, such as level walking, transverse walking, and turning. These findings suggest that distinguishing activities with overlapping kinematic features using a single IMU remains a challenging task. The chattering behavior in the error profiles in Figs. 8 and 9 does not indicate poor performance but rather reflects the inherent sensitivity of error calculations. This behavior might arise from noise in the IMU signals, which can be amplified when predicting high-dimensional outputs like joint angles. In such cases, small inaccuracies in IMU measurements might propagate through the model, resulting in oscillations in the predicted angles. Despite this, the actual predicted angles closely align with the ground truth, and the overall trends and mean errors remain well within acceptable ranges.

As shown in Fig. 8, in contrast to the slope angle ϕ, the turning angle ψ predictions exhibit slightly larger variability throughout the gait cycle. This can be attributed to the complex nature of turning movements, which involve multiple degrees of freedom and can be influenced by factors such as walking speed, stride length, and individual gait characteristics. It is worth noting that the largest turning angle errors occurred when the subjects' facing directions align with the X-axis. The system might have difficulty accurately capturing the turning angles during these specific orientations. Despite these challenges, the overall turning angle prediction accuracy remains reasonably high. The prediction errors for slope and turning angles (Fig. 8) demonstrate the model's consistency across trained angles. The slightly increased variability in untrained slopes indicates that while the model exhibits generalization capability, there exists room to improve its ability to handle conditions beyond the training scope. Expanding the training data set to include a broader range of gait conditions or employing transfer learning techniques could potentially enhance the performance.

The proposed approach demonstrates superior performance in joint angle estimation, with the lowest RMSE as 1.17 deg for the elbow joint. This level of accuracy is particularly impressive when compared to the overall error of approximately 16 deg for joint angle reconstruction in various non-walking 3D human motions using multiple IMUs that was reported in [41]. The gait motion considered in this study is periodic and this may contribute to the higher accuracy achieved by the proposed method. Nevertheless, the findings confirm that a single IMU-based approach achieves a level of accuracy commensurate with multi-IMU systems for human walking posture estimation. The knee joint exhibited a higher RMSE compared to upper-limb joints due to its greater biomechanical complexity, its crucial role in stabilization and adaptation on sloped terrains, and the increased variability of knee motion in such conditions, as demonstrated in previous studies [42]. Soft tissue artifacts and vibrations, which tend to be pronounced in lower-limb IMU readings, contribute to noise in knee angle predictions. Given the knee's large range of motion, even small relative errors result in high RMSE values, as reflected in Table II.

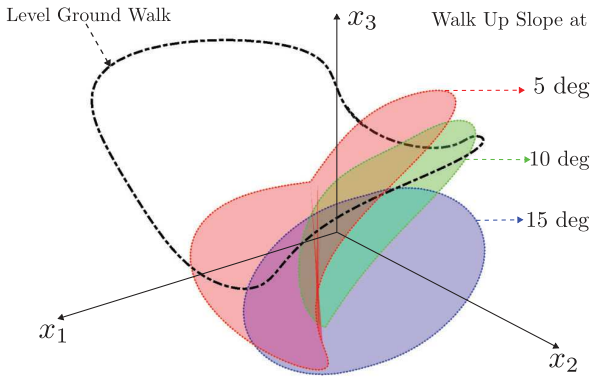

Fig. 10. Averaged GPDM latent space manifolds of walking on different slopes. The manifolds represent the GPDM-embedded gait dynamics on level ground and slopes with $\phi = 5, 10, 15$ deg. Each trajectory depicts a continuous evolution of the gait cycle in the latent space, illustrating the model's ability to distinguish gait patterns between different slope inclinations.

One advantage of the used GPDM for posture estimation lies in its representation in low-dimensional space. We took the latent space dimension $d = 3$ and the dimension of the joint angle space was $D = 12$ in this study. Fig. 10 shows the motion trajectory in the latent space for walking activities at level ground and at slope angles of $\phi = 5, 10, 15$ deg. The distinct and non-intersecting surfaces represent the manifold of each activity, highlighting the model's ability to distinguish walking gaits across different slopes. The clear separation among these manifolds validates the GPDM's capacity for interpolating latent states for untrained slopes.

The proposed work has significant real-world implications, particularly in construction where monitoring workers' gait and posture is critical for ensuring work safety and productivity. The developed system has the potential to be integrated into existing workflows and technologies, enabling real-time monitoring and feedback to prevent work-related injuries and improve ergonomics. By providing accurate and timely information on workers' gait, posture, and floor slope angles, the system can contribute to the development of personalized assistive robotics, training programs, and safety protocols [20], [23]. Furthermore, the real-time nature of the system allows for prompt detection of potential hazards or deviations from safe

working practices, enabling timely corrective or intervention actions.

While the proposed approach demonstrates promising outcomes, there remain several areas for further development and enhancement. The proposed methodology is primarily suited for walking gait and might not fully capture the complexities of non-periodic or irregular human movements often encountered in daily activities in construction. Moreover, the increased error during transitions between different types of activities underscores the need for further improvements in capturing these crucial moments for comprehensive human motion understanding. Additionally, the joint angle estimation in this study focused on steady-state walking on level and sloped floors, excluding many other work activities in construction such as stair walking. Extending the model to include ascent and descent stair climbing, similar to the work in [14] and [22], as well as other gaits, such as squatting and kneeling, could broaden its applicability. Finally, the experiment study in this work used healthy, young participants who were selected from university student population. Although inter-subject variability in walking gait is not significant, it is desirable to conduct additional experiments and validate the method with construction workers or professionals.

VII. Conclusion

This paper presented a real-time walking gait prediction and posture estimation method for construction workers on level and sloped floors. A combination of the LSTM-based network and the GPDM was mainly used in the estimation scheme. The walking activities were predicted, the slope angle and turning angle were estimated, and human pose was predicted in real time with relatively low average joint angle errors. The experimental results demonstrated the effectiveness and efficacy of the walking activity detection and posture estimation design. A key attractive of the proposed scheme was the real-time capability with 21 ms latency using a single IMU attached to the distal portion of the right shank. We are currently working on improving the real-time performance and also integrating the design with wearable assistive robotic devices for construction workers (e.g., [20], [23]).

References

[1] C. R. Ahn, S. Lee, C. Sun, H. Jebelli, K. Yang, and B. Choi, "Wearable sensing technology applications in construction safety and health," *J. Construct. Eng. Manage.*, vol. 145, no. 11, Nov. 2019, Art. no. 03119007.

[2] E. Valero, A. Sivanathan, F. Bosché, and M. Abdel-Wahab, "Musculoskeletal disorders in construction: A review and a novel system for activity tracking with body area network," *Appl. Ergonom.*, vol. 54, pp. 120–130, May 2016.

[3] W. Supanich, S. Kulkarineetham, P. Sukphokha, and P. Wisarnsart, "Machine learning-based exercise posture recognition system using MediaPipe pose estimation framework," in *Proc. 9th Int. Conf. Adv. Comput. Commun. Syst. (ICACCS)*, vol. 1, Coimbatore, India, Mar. 2023, pp. 2003–2007.

[4] Q. Mascret, G. Gagnon-Turcotte, M. Bielmann, C. L. Fall, L. J. Bouyer, and B. Gosselin, "A wearable sensor network with embedded machine learning for real-time motion analysis and complex posture detection," *IEEE Sensors J.*, vol. 22, no. 8, pp. 7868–7876, Apr. 2022.

[5] S. S. Bangaru, C. Wang, and F. Aghazadeh, "Data quality and reliability assessment of wearable EMG and IMU sensor for construction activity recognition," *Sensors*, vol. 20, no. 18, p. 5264, Sep. 2020.

[6] X. Yan, H. Li, A. R. Li, and H. Zhang, "Wearable IMU-based real-time motion warning system for construction workers' musculoskeletal disorders prevention," *Autom. Construct.*, vol. 74, pp. 2–11, Feb. 2017.

[7] E. Valero, A. Sivanathan, F. Bosché, and M. Abdel-Wahab, "Analysis of construction trade worker body motions using a wearable and wireless motion sensor network," *Autom. Construct.*, vol. 83, pp. 48–55, Nov. 2017.

[8] A. Alwasel, A. Sabet, M. Nahangi, C. T. Haas, and E. Abdel-Rahman, "Identifying poses of safe and productive masons using machine learning," *Autom. Construct.*, vol. 84, pp. 345–355, Dec. 2017.

[9] G. P. Panebianco, M. C. Bisi, R. Stagni, and S. Fantozzi, "Analysis of the performance of 17 algorithms from a systematic review: Influence of sensor position, analysed variable and computational approach in gait timing estimation from IMU measurements," *Gait Posture*, vol. 66, pp. 76–82, Oct. 2018.

[10] J. Lee, H. Joo, J. Lee, and Y. Chee, "Automatic classification of squat posture using inertial sensors: Deep learning approach," *Sensors*, vol. 20, no. 2, p. 361, Jan. 2020.

[11] P. F. Hendriksen, M. Korshøj, J. Skotte, and A. Holtermann, "Detection of kneeling and squatting during work using wireless triaxial accelerometers," *Ergonomics*, vol. 63, no. 5, pp. 607–617, May 2020.

[12] M. Trkov, K. Chen, J. Yi, and T. Liu, "Inertial sensor-based slip detection in human walking," *IEEE Trans. Autom. Sci. Eng.*, vol. 16, no. 3, pp. 1399–1411, Jul. 2019.

[13] C. Zhu and J. Yi, "Knee exoskeleton-enabled balance control of human walking gait with unexpected foot slip," *IEEE Robot. Autom. Lett.*, vol. 8, no. 11, pp. 7751–7758, Nov. 2023.

[14] G. Zuo, Q. Wu, W. Gao, C. Li, L. Sun, and S. Yu, "Accurate and real-time hierarchical ensemble network for activity classification in construction worker," *IEEE J. Biomed. Health Informat.*, early access, Apr. 16, 2025, doi: 10.1109/JBHI.2025.3561380.

[15] J. Figueiredo, P. Félix, L. Costa, J. C. Moreno, and C. P. Santos, "Gait event detection in controlled and real-life situations: Repeated measures from healthy subjects," *IEEE Trans. Neural Syst. Rehabil. Eng.*, vol. 26, no. 10, pp. 1945–1956, Oct. 2018.

[16] Y. Huang et al., "Real-time intended knee joint motion prediction by deep-recurrent neural networks," *IEEE Sensors J.*, vol. 19, no. 23, pp. 11503–11509, Dec. 2019.

[17] I. Kang, P. Kunapuli, and A. J. Young, "Real-time neural network-based gait phase estimation using a robotic hip exoskeleton," *IEEE Trans. Med. Robot. Bionics*, vol. 2, no. 1, pp. 28–37, Feb. 2020.

[18] C. Zhu, F. Han, and J. Yi, "Wearable sensing and knee exoskeleton control for awkward gaits assistance," in *Proc. IEEE 18th Int. Conf. Autom. Sci. Eng. (CASE)*, Mexico city, Mexico, Aug. 2022, pp. 2393–2398.

[19] T. Yigit, F. Han, E. Rankins, J. Yi, K. H. McKeever, and K. Malinowski, "Wearable inertial sensor-based limb lameness detection and pose estimation for horses," *IEEE Trans. Autom. Sci. Eng.*, vol. 19, no. 3, pp. 1365–1379, Jul. 2022.

[20] G. Sreenivasan, C. Zhu, and J. Yi, "Exoskeleton-assisted stance and kneeling balance and work task evaluation in construction," *IEEE Trans. Autom. Sci. Eng.*, early access, Feb. 4, 2025, doi: 10.1109/TASE.2025.3538532.

[21] S. Yu et al., "Quasi-direct drive actuation for a lightweight hip exoskeleton with high backdrivability and high bandwidth," *IEEE/ASME Trans. Mechatronics*, vol. 25, no. 4, pp. 1794–1802, Aug. 2020.

[22] D. Lee, I. Kang, D. D. Molinaro, A. Yu, and A. J. Young, "Real-time user-independent slope prediction using deep learning for modulation of robotic knee exoskeleton assistance," *IEEE Robot. Autom. Lett.*, vol. 6, no. 2, pp. 3995–4000, Apr. 2021.

[23] S. Chen et al., "Wearable knee assistive devices for kneeling tasks in construction," *IEEE/ASME Trans. Mechatronics*, vol. 26, no. 4, pp. 1989–1996, Aug. 2021.

[24] J. Camargo, W. Flanagan, N. Csomay-Shanklin, B. Kanwar, and A. Young, "A machine learning strategy for locomotion classification and parameter estimation using fusion of wearable sensors," *IEEE Trans. Biomed. Eng.*, vol. 68, no. 5, pp. 1569–1578, May 2021.

[25] H. M. Balaha and A. E.-S. Hassan, "Comprehensive machine and deep learning analysis of sensor-based human activity recognition," *Neural Comput. Appl.*, vol. 35, no. 17, pp. 12793–12831, Jun. 2023.

[26] C. Zheng et al., "Deep learning-based human pose estimation: A survey," *ACM Comput. Surv.*, vol. 56, no. 1, pp. 1–37, 2023.

[27] Mst. A. Khatun et al., "Deep CNN-LSTM with self-attention model for human activity recognition using wearable sensor," *IEEE J. Transl. Eng. Health Med.*, vol. 10, 2022, Art. no. 2700316.

[28] K. Lee, W. Kim, and S. Lee, "From human pose similarity metric to 3D human pose estimator: Temporal propagating LSTM networks," *IEEE Trans. Pattern Anal. Mach. Intell.*, vol. 45, no. 2, pp. 1781–1797, Feb. 2023.
[29] K. Holmquist and B. Wandt, "DiffPose: Multi-hypothesis human pose estimation using diffusion models," in *Proc. IEEE/CVF Int. Conf. Comput. Vis. (ICCV)*, Oct. 2023, pp. 15931–15941.
[30] W. Shan et al., "Diffusion-based 3D human pose estimation with multi-hypothesis aggregation," in *Proc. IEEE/CVF Int. Conf. Comput. Vis. (ICCV)*, Oct. 2023, pp. 14715–14725.
[31] N. Gaud, M. Rathore, and U. Suman, "MHCNLS-HAR: Multiheaded CNN-LSTM-based human activity recognition leveraging a novel wearable edge device for elderly health care," *IEEE Sensors J.*, vol. 24, no. 21, pp. 35394–35405, Nov. 2024.
[32] N. Kumari, A. Yadagani, B. Behera, V. B. Semwal, and S. Mohanty, "Human motion activity recognition and pattern analysis using compressed deep neural networks," *Comput. Methods Biomechanics Biomed. Engineering: Imag. Visualizat.*, vol. 12, no. 1, Dec. 2024, Art. no. 2331052.
[33] K. Chen, Y. Zhang, J. Yi, and T. Liu, "An integrated physical-learning model of physical human–robot interactions with application to pose estimation in bikebot riding," *Int. J. Robot. Res.*, vol. 35, no. 12, pp. 1459–1476, Apr. 2016.
[34] D. Holden, T. Komura, and J. Saito, "Phase-functioned neural networks for character control," *ACM Trans. Graph.*, vol. 36, no. 4, pp. 1–13, Aug. 2017.
[35] S. Chen, S. S. Bangaru, T. Yigit, M. Trkov, C. Wang, and J. Yi, "Real-time walking gait estimation for construction workers using a single wearable inertial measurement unit (IMU)," in *Proc. IEEE/ASME Int. Conf. Adv. Intell. Mechatronics (AIM)*, Jul. 2021, pp. 753–758.
[36] K. Kim and Y. K. Cho, "Effective inertial sensor quantity and locations on a body for deep learning-based worker's motion recognition," *Autom. Construct.*, vol. 113, May 2020, Art. no. 103126.
[37] N. D. Lawrence and J. Quiñonero-Candela, "Local distance preservation in the GP-LVM through back constraints," in *Proc. 23rd Int. Conf. Mach. Learn.*, Pittsburgh, PA, USA, 2006, pp. 513–520.
[38] J. Y. Maldonado-Contreras, K. Bhakta, J. Camargo, P. Kunapuli, and A. J. Young, "User-and speed-independent slope estimation for lower-extremity wearable robots," *Ann. Biomed. Eng.*, vol. 52, pp. 1–11, Nov. 2023.
[39] I. Kang, P. Kunapuli, H. Hsu, and A. J. Young, "Electromyography (EMG) signal contributions in speed and slope estimation using robotic exoskeletons," in *Proc. IEEE 16th Int. Conf. Rehabil. Robot. (ICORR)*, Jun. 2019, pp. 548–553.
[40] J. Camargo, A. Ramanathan, W. Flanagan, and A. Young, "A comprehensive, open-source dataset of lower limb biomechanics in multiple conditions of stairs, ramps, and level-ground ambulation and transitions," *J. Biomechanics*, vol. 119, Apr. 2021, Art. no. 110320.
[41] Y. Huang, M. Kaufmann, E. Aksan, M. J. Black, O. Hilliges, and G. Pons-Moll, "Deep inertial poser: Learning to reconstruct human pose from sparse inertial measurements in real time," *ACM Trans. Graph.*, vol. 37, no. 6, pp. 1–15, Dec. 2018.
[42] J. Sarvestan, P. A. Ataabadi, F. Yazdanbakhsh, S. Abbasi, A. Abbasi, and Z. Svoboda, "Lower limb joint angles and their variability during uphill walking," *Gait Posture*, vol. 90, pp. 434–440, Oct. 2021.

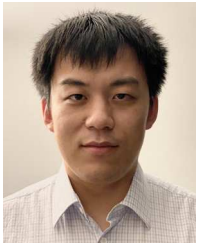

Siyu Chen received the B.S. and M.S. degrees in mechanical engineering from the Huazhong University of Science and Technology, China, in 2011 and 2014, respectively, and the Ph.D. degree in mechanical and aerospace engineering from Rutgers University, USA, in 2022. Since then, he has been at MathWorks, Inc., continuing his work in engineering and applied research. His research interests include control and learning algorithms for autonomous and mechatronic systems, physical human-robot interaction, and dynamic robotic systems.

Chunchu Zhu (Student Member, IEEE) received the B.E. degree in mechanical engineering from the Southern University of Science and Technology, Shenzhen, China, in 2019, and the M.S. degree in mechanical engineering from Case Western Reserve University, Cleveland, OH, USA, in 2021. He is currently pursuing the Ph.D. degree in mechanical and aerospace engineering with Rutgers University, NJ, USA.

His research interests include dynamics, control, and machine learning, with applications to human-robot interaction, rehabilitation robotics, and biomechanical modeling.

Xunjie Chen (Student Member, IEEE) received the B.S. degree in vehicle engineering from Jilin University, Changchun, China, in 2018, and the M.Eng. degree in vehicle engineering from Tongji University, Shanghai, China, in 2021. He is currently pursuing the Ph.D. degree in mechanical and aerospace engineering with Rutgers University, Piscataway, NJ, USA.

His research interests include dynamic systems and control, modeling and control for bipedal robotics, and mechatronics.

Jingang Yi (Senior Member, IEEE) received the B.S. degree in electrical engineering from Zhejiang University, Hangzhou, China, in 1993, the M.Eng. degree in precision instruments from Tsinghua University, Beijing, China, in 1996, and the M.A. degree in mathematics and the Ph.D. degree in mechanical engineering from the University of California at Berkeley, Berkeley, CA, USA, in 2001 and 2002, respectively.

He is currently a Professor of Mechanical Engineering and a Peter D. Cherasia Faculty Scholar at Rutgers University. His research interests include autonomous robotic systems, dynamic systems and control, mechatronics, automation science, and engineering, with applications to biomedical systems, civil infrastructure, and transportation systems. He is a fellow of American Society of Mechanical Engineers (ASME). He was a recipient of the 2010 US NSF CAREER Award. He serves as a Senior Editor for IEEE TRANSACTIONS ON AUTOMATION SCIENCE AND ENGINEERING and an Associate Editor for *International Journal of Intelligent Robotics and Applications*. He served as a Senior Editor for IEEE ROBOTICS AND AUTOMATION LETTERS and an Associate Editor for IEEE TRANSACTIONS ON AUTOMATION SCIENCE AND ENGINEERING, IEEE/ASME TRANSACTIONS ON MECHATRONICS, IEEE ROBOTICS AND AUTOMATION LETTERS, *IFAC Journal Mechatronics*, *Control Engineering Practice*, and *ASME Journal of Dynamic Systems, Measurement and Control*.